Chapter 3: Microstructure and Mechanical Properties of Austenitic Low-Density Steel

3.1 Introduction

An austenitic low-density steel (P1) (Fe-18Mn-6.5Al-0.75C) is produced using vacuum induction melting, followed by hot rolling and solution treatment to achieve a single-phase austenite structure (PD1-S). Results of the microstructure and mechanical properties, as well as the effects of cold rolling and repeated annealing treatments on the selected alloy are reported in the Chapter 3. Additionally, the influence of strain rate on tensile properties is examined.

3.2 Results

3.2.1 Phase diagram

Calculated phase diagram of selected alloy (Figure 3.1) obtained through ThermoCalc software delineates the phase stability regions as a function of temperature and aluminum concentration, under constant concentrations for 18Mn-0.75C. The austenite phase exhibits thermodynamic stability at an aluminum concentration of 6.2 mass %, within the temperature range of 650°C to 1240°C.

When the selected alloy as indicated by red broken line (Figure 3.1) is cooled from the liquid state, the sequence of phase transformations involved as per the calculated phase diagram are given by the following steps;

(1) Liquid (> 1421 °C) → (2) Liquid+δ-ferrite (BCC_A2) (1421 °C - 1345 °C) → (3) δ-ferrite (BCC_A2) + Austenite (FCC_A1) (1345 °C - 1240 °C) → (4) Austenite (FCC_A1) (1240 °C - 650 °C) → (5) Austenite (FCC_A1) + K-carbide (KAPPA_E21) (650 °C - 600

°C) → (6) Austenite (FCC_A1)+ K-carbide (KAPPA_E21)+ α-ferrite (BCC_A2) (600 °C - 500 °C) → (7) Austenite (FCC_A1)+ K-carbide (KAPPA_E21) + α-ferrite (BCC_A2) +$M_{23}C_6$_D84 (500 °C - 420 °C) → (8) k-carbide (KAPPA_E21) + α-ferrite (BCC_A2)+ $M_{23}C_6$_D84 (420 °C - 336 °C) → (9) K-carbide (KAPPA_E21) + α-ferrite (BCC_A2) +$M_{23}C_6$_D84+BCC_B2#2 (336 °C - 52 °C) → (10) K-carbide (KAPPA_E21) + α-ferrite (BCC_A2) +$M_{23}C_6$_D84+BCC_B2#2 + BCC_B2#3 + FCC_L1_2 (52 °C – 0°C).

In addition, there are 3 more phases existing in other compositions in the diagram, these phases are CUB_A12, CUB_A13 and Cementite_D011, which are α-Mn, β-Mn and Fe3C, respectively.

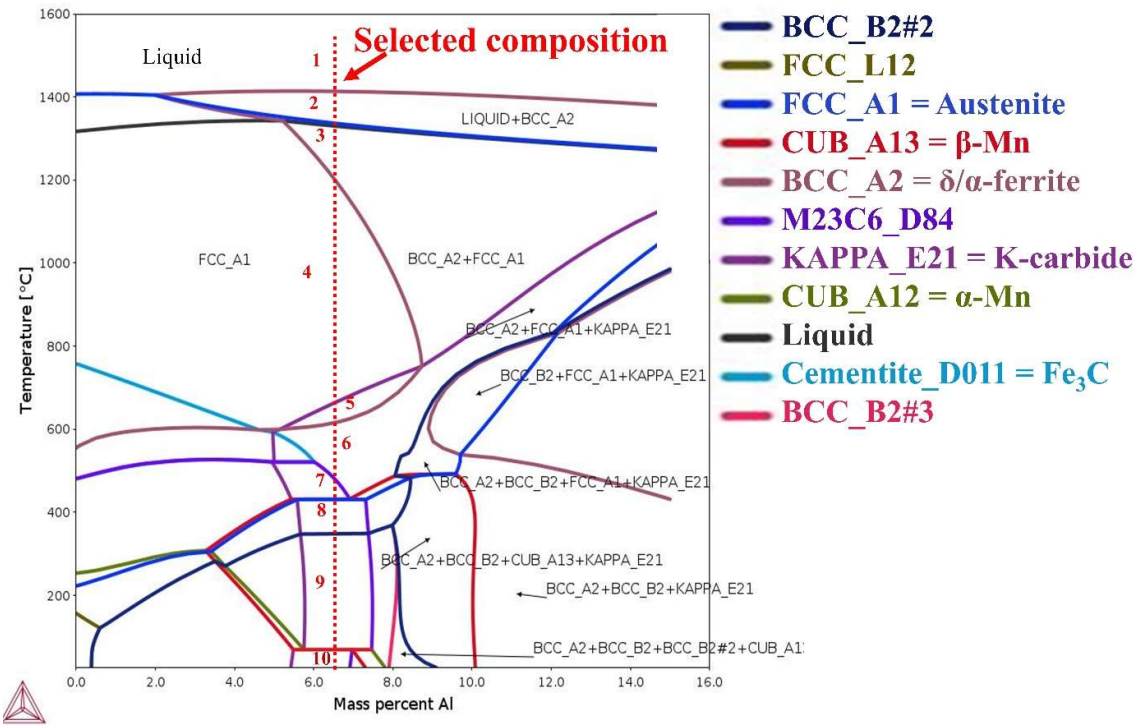

Figure 3.1: Calculated phase diagram of selected alloy using ThermoCalc software, illustrating phase stability regions as a function of temperature and aluminum concentration.

3.2.2 Physical properties

The density of PD1-S is 6.99± 0.03 g/cc, as determined using Archimedes' principle. The values of the elastic modulus, shear modulus, and Poisson's ratio obtained through ultrasonic testing of the sample, are 169± 0.45 GPa, 65.53 GPa, and 0.29, respectively, and presented in Table 3.1.

Table 3.1: Density, Elastic modulus, Shear modulus, and Poisson ratio of PD1-S steel.

Density (g/cc)	Longitudinal velocity (m/s)	Transverse velocity (m/s)	Poisson ratio	Shear modulus (GPa)	Elastic modulus (GPa)
6.99± 0.03	5649 ± 20.3	3063 ± 18.2	0.29	65.5	169± 0.45

3.2.3 Microstructural Characterization

The optical microstructure of the PD1-S sample reveals austenite grains with an average size of 53 ± 18 μm, accompanied by characteristic annealing twins as displayed in Figure 3.2 (a). The XRD analysis confirms that the PD1-S sample consists of austenite, with peaks corresponding to the (111), (200), (220), (311), and (222) planes (Figure 3.2 (b)). The micro-strain and dislocation density values for the PD1-S sample are calculated to be 0.00058 and 3.6×10^{13} m^{-2}, respectively. The image quality (IQ) map obtained from EBSD analysis reveals distinct annealing twins (Figure 3.3 (a)). Based on grain size versus area fraction chart (shown in Figure 3.3 (b)), the average grain size of austenite is calculated to be 82.6 ± 8.9 μm. Observations from both the optical micrograph and the IQ map indicate some variation in grain size, likely due to the limited area covered in the EBSD scan.

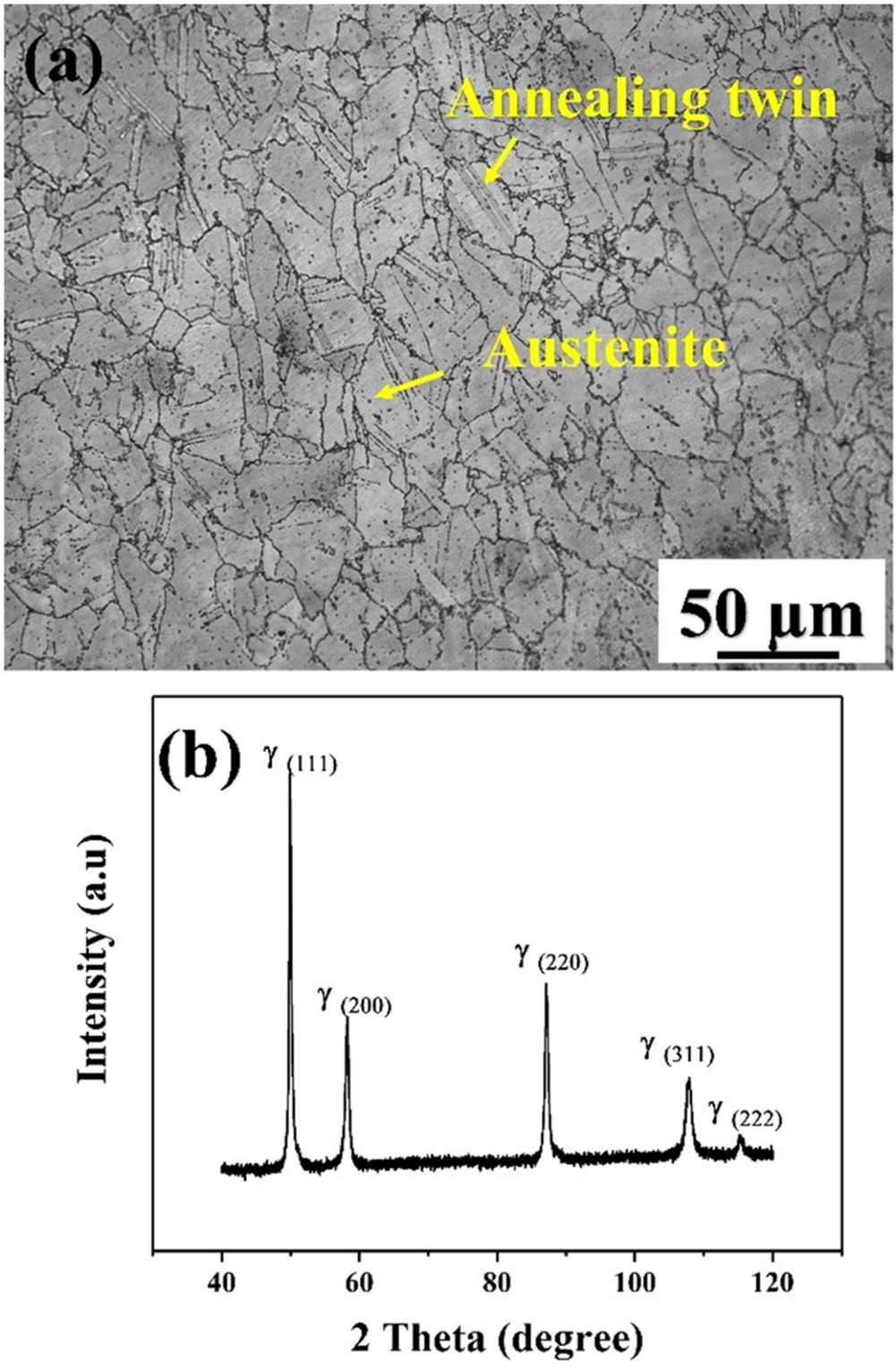

Figure 3.2: (a) Optical micrograph (b) XRD pattern of PD1-S.

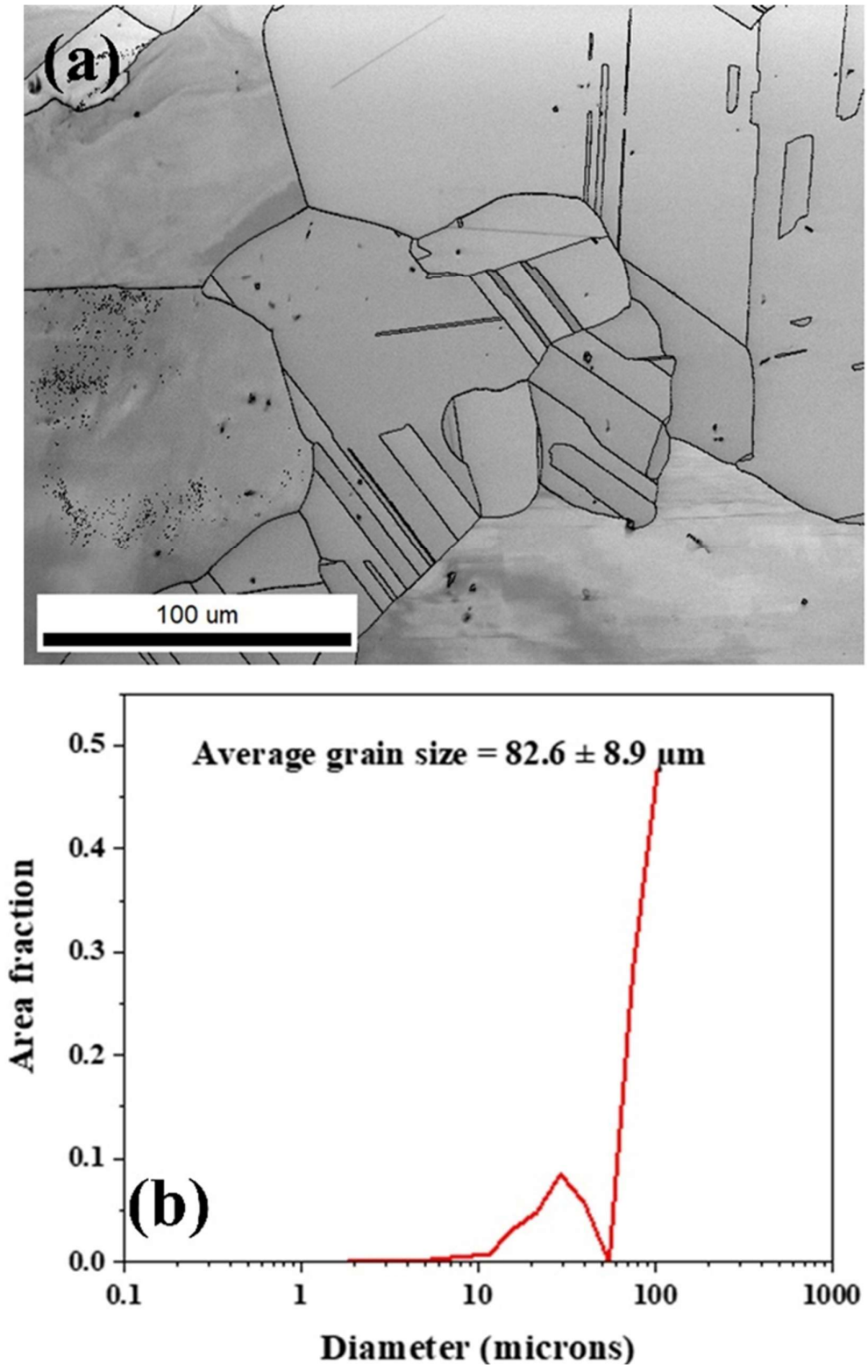

Figure 3.3: (a) IQ map (b) Grain size vs area fraction chart of PD1-S.

3.2.4 Tensile properties

The engineering stress-strain curve and corresponding fractograph of PD1-S are shown in Figure 3.4 (a) and Figure 3.4 (b), respectively. PD1-S exhibited a yield strength (YS) of 435 ± 7 MPa, an ultimate tensile strength (UTS) of 732 ± 10 MPa, and a total elongation (T.E.) of 58.8 ± 2%. The UTS/YS ratio for PD1-S was calculated to be 1.68. SEM fractography of the tensile-tested PD1-S specimens reveals primarily dimple features with an average size of 8.7 ± 1.7 μm, accompanied by tearing ridges, indicating a predominantly ductile fracture mode due to micro void coalescence.

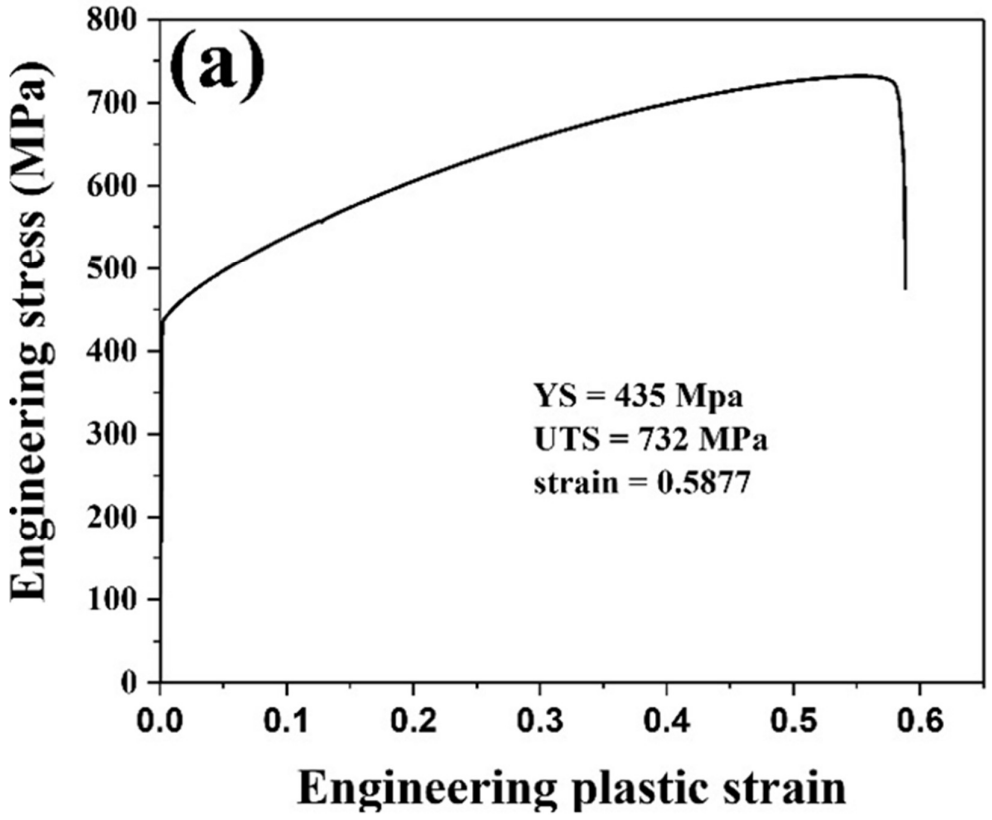

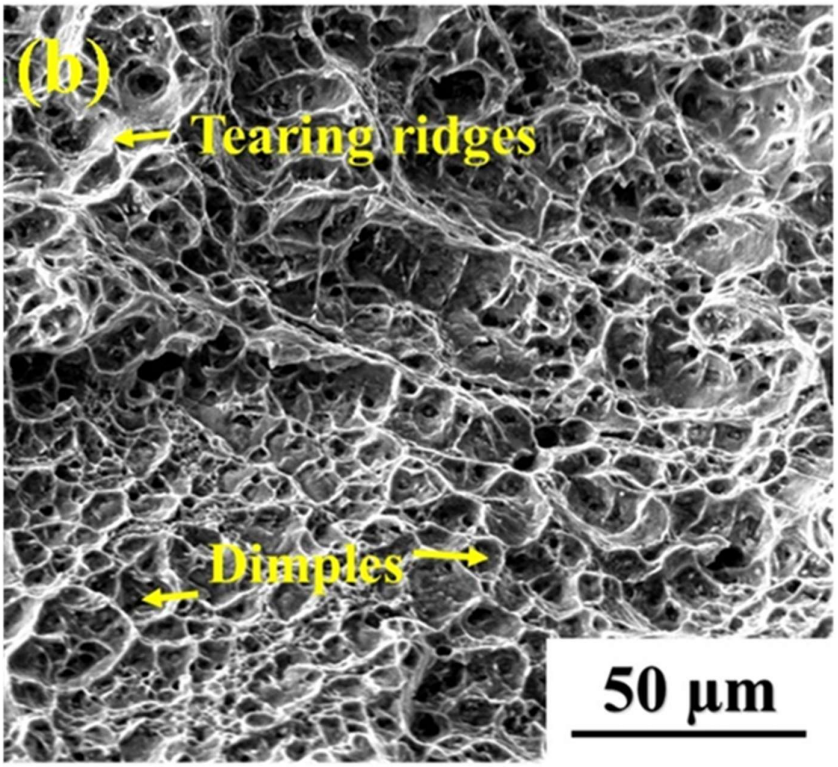

Figure 3.4: (a) Engineering stress-strain curve of PD1-S and its (b) SEM fractograph.

3.3 Discussion

The addition of aluminum causes a reduction in density of ~8% for PD1-S. The remaining ~5% reduction in density is mainly attributed to high concentrations of C [11]. Existing literature suggests that the introduction of only 1 mass% of aluminum can result in a decrease in the elastic modulus of approximately 2-2.5% [20]. As a consequence, it is anticipated that the elastic modulus of PD1-S will decrease by approximately 12-15%. The measured elastic modulus values for PD1-S exhibit a decrease of 11% compared to the that of steels without aluminum, aligning closely with the existing literature [20]. The optical micrograph and XRD patterns of PD1-S confirm the presence of a single austenite phase, with larger grain sizes attributed to higher processing temperatures and the absence of precipitates at grain boundaries. According to equilibrium phase diagrams, PD1-S consists entirely of austenite at solutionising temperature of 950 °C. There is a possibility of

formation of FeAl in Fe-Mn-Al-C system of selected composition at around 350°C under slow cooling/equilibrium conditions. In the present case, the alloy has undergone non equilibrium processings of homogenization (1050 °C), hot rolling (1050 °C – 950 °C), solutionising at high temperature (950°C) followed by quenching in water at room temperature. There is very little chance of FeAl formation.

3.3.1 Strengthening mechanisms and its contribution to yield strength

The yield strength (σ_γ) of austenite in PD1-S can be calculated using Equation 3.1 [50].

$$\sigma_\gamma = \sigma_P + \sigma_D + \sigma_{SS} + \sigma_{GB} \quad [3.1]$$

Where σ_P is Peierls stress, σ_D is dislocation strengthening, σ_{SS} is solid solution strengthening, and σ_{GB} is grain boundary strengthening, respectively.

The Peierls stress σ_P is given by $3\tau_0$ [116],where τ_0 is shear stress which is $2*10^{-4}G$ [117]. Here G is the shear modulus. Taking respective G value as 65.5 GPa for PD1-S, the Peierls stress is calculated to be 39.3 MPa (Table 3.2).

σ_D is determined using Taylor expression as given in Equation 3.2 [118].

$$\sigma_D = M\alpha Gb\sqrt{\rho} \quad [3.2]$$

Here, M is the Taylor factor of austenite (i.e., 3.1, calculated from EBSD data), $\alpha\ is$ Taylor constant (0.24) [119], b as Burger vector which is 2.6 Å (calculated from XRD data). The calculated σ_D is found to be 76 MPa (Table 3.2).

σ_{SS} is estimated by using the Equation 3.3 [120].

$$\sigma_{SS} = 279 * wt.\%C - 1.5 * wt.\%Mn + 20.5 * wt.\%\ Al \quad [3.3]$$

The estimated σ_{SS} for PD1-S is 306 MPa.

The grain boundary contribution to yield strength (σ_{GB}) is calculated using Hall-Petch relation and is given by Equation 3.4 [121].

$$\sigma_{GB} = K_B . d^{-1/2} \quad [3.4]$$

where K_B is grain boundary locking parameter, which is taken as 330 MPa.µm1/2 for similar low-density steel [78] and d is grain size of austenite which is 53 µm for PD1-S. The estimated σ_{GB} value for PD1-S is 45.3 MPa (Table 3.2).

Therefore, the yield strength (σ_γ) of austenite of PD1-S is calculated to be 466.6 MPa (Table 3.2) which is overestimated by 31.6 MPa. The error in estimation may be due to variation in grain size, and its distribution. Solid solution strengthening is the primary mechanism for strengthening due to the presence of higher amounts of alloying elements.

Table 3.2: Strengthening contributions from various mechanisms to yield strength.

Strengthening mechanism	σ_P	σ_{SS}	σ_D	σ_{GB}	Calculated YS	Experimental YS
Contribution to YS (MPa)	39.3	306	76	45.3	466.6	435

3.3.2 Work hardening behavior

The logarithmic true stress versus logarithmic true plastic strain plots for PD1-S fitted with Hollomon [109], Ludwik [110], Ludwigson [112], Swift [111], and Voce [113] flow models are presented in Figure 3.5 (a). The slopes or work hardening rates undergo two types of changes: one at low strain, and another at high strain, with a transition occurring at intermediate strain. Out of the considered models, the Ludwigson relationship is found to be the best fit for the experimental data with the highest R^2 (coefficient of determination)

value and the lowest χ^2 (sum of squares of deviation of calculated stress values from experimental stress values) values of 0.99968 and 5.25 MPa^2 respectively.

Ludwigson flow behavior is given by Equation 3.5.

$$\sigma = exp(K_1 + n_1\varepsilon) + K\varepsilon^n \quad [3.5]$$

Where $\exp(K_1)$ and K are strength coefficients and n_1, and n are work-hardening exponents, respectively, at low and high strain regimes [122].

The strength coefficient (K_1) of PD1-S in low-strain regimes is 441 MPa (Table 3.3). The corresponding work-hardening exponent (n_1) is 0.02. In high strain regimes, PD1-S exhibits a higher strength coefficient (K) value of 1602 MPa and work hardening exponent (n) value of 1.02.

The differentiation of the Ludwigson equation with respect to strain yields Equation 3.6, which quantifies the variations in the work hardening rate.

$$\frac{d\sigma}{d\varepsilon} = n_1 \exp(K_1 + n_1\varepsilon) + Kn\varepsilon^{n-1} \quad [3.6]$$

Equation 3.6 indicates the existence of two distinct variations in work hardening rate relative to true strain.

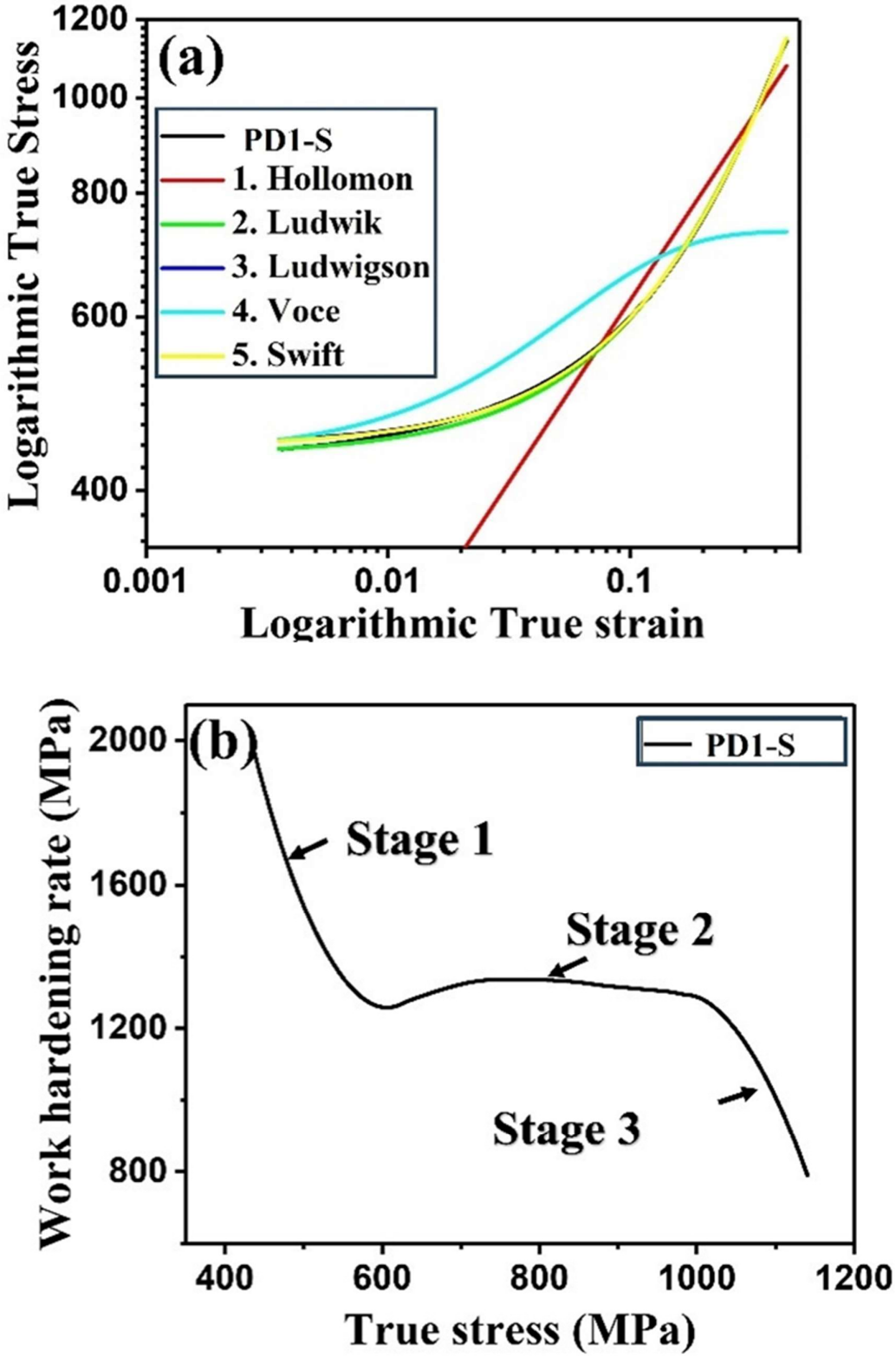

Figure 3.5: (a) Logarithmic true stress vs. logarithmic true plastic strain plots of PD1-S fitted with various models, (b) Work hardening rate vs true plastic stress diagram.

Table 3.3: Strength coefficients, work-hardening exponents and fitting parameters with Ludwigson flow equation for PD1-S.

Steel	exp(K_1) (MPa)	n_1	K (MPa)	n	R^2	χ^2
PD1-S	441	0.02	1602	1.02	0.9998	5.25

The experimental work hardening rate variation in relation to true plastic stress for PD1-S during three stages (Stage 1-Stage 3) is depicted in Figure 3.5 (b). The initial stage demonstrates a pronounced decline in the work hardening rate. In Stage 2, there is a slight increase in the work hardening rate, followed by a subsequent decline with a relatively constant slope. Stage 3 is characterized by a dynamic recovery.

At a low-stress regime, the work hardening rate decreases rapidly with gradients of -4 (approximately 400-600 MPa). Stage 1, also referred to as the easy glide stage, primarily occurs due to the planar flow of dislocations (planar slip) over long distances, where the motion of dislocations is hindered by minimal obstacles like precipitates or grain boundaries [123]. The rate of accumulation of dislocations is negligible in this stage.

At higher stress regimes, the work hardening rate of PD1-S (725-1025 MPa) decreases gradually. The gradients of the work hardening rate with respect to true stress is -0.19. From true stress range, 600-725 MPa, there is an increase in the work hardening rate with a gradient of 0.65. This observed increase may be attributed to the refinement of dynamic slip bands [124]. The activation of cross-slip and multiple-slip systems enhances the formation of heterogeneous dislocation structures comprising dislocation tangles, walls, and cells. The proportion of these structures increases as the plastic strain during stage 2 progresses [125]. Stage 2 corresponds to the phase of enhanced dislocation storage, characterized by the proliferation of wall and cell structures, resulting in an increase in dislocation density.

Stage 3 represents the dynamic recovery phase, wherein dislocations undergo annihilation, leading to a reduction in the work hardening rate. The linear relationship observed between the hardening rate ($\frac{d\sigma}{d\epsilon_p}$) and true plastic stress (σ) curves in the third stage (Figure 3.6) can be most effectively elucidated similar to the Kock, Mecking, (KM) dislocation models [118], [126], as expressed in Equation 3.7.

$$\frac{d\sigma}{d\epsilon} = \theta_0 + m\sigma \quad [3.7]$$

Here, $\frac{d\sigma}{d\epsilon}$ and σ represent the strain hardening rate and the true stress, respectively. The initial work-hardening rate, denoted as θ_0, signifies the athermal mobility of dislocation storage that has been arrested following a proportional travel distance relative to the average slip spacing. The term m correspondingly refers to the gradient of the linear regimes attributed to the elimination of dislocations caused by cross slip during dynamic recovery [127]. A high value of θ_0 indicates a high dislocation storage capacity signifying the material's ability to retain dislocations. Conversely, a high negative value of m suggests high dynamic recovery implying that the material experiences work softening.

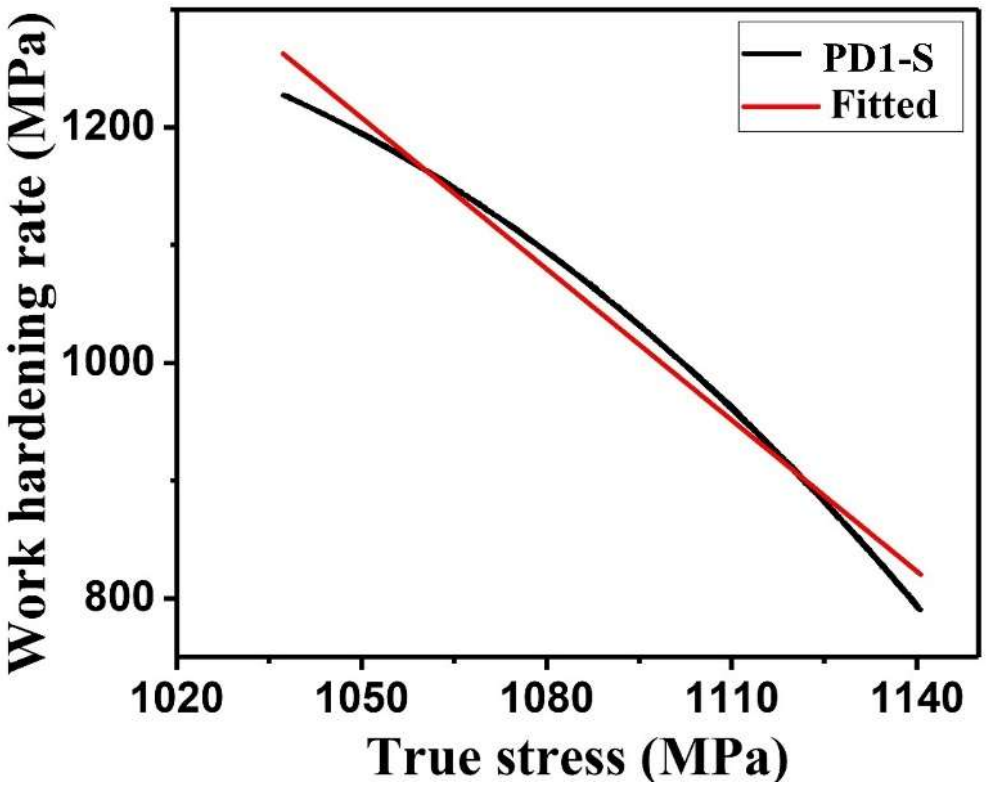

Figure 3.6: Linear fitting curves of the third stage in PD1-S using Kock, Mecking, (KM) based dislocation models.

The adjusted R^2 value of the fitted curves approaches 1, indicating a strong correlation between the experimental data and the fitted curve. The dislocation storage capacity (θ_0) of PD1-S is determined to be 5699 MPa. Conversely, the negative slope (m) of the curve for PD1-S is observed to be -4.

The material exhibited strength and ductility values greater than 30 GPa % (the minimum requirement for third-generation advanced high-strength steels), with values of 43 GPa % for PD1-S. The specific stiffness ($\frac{E}{\rho}$) values for PD1-S is calculated to be 24.1 MPa. m^3/ kg.

3.4 Effect of cold rolling and repeated annealing (Thermal cyclic treatment)

3.4.1 Results

3.4.1.1 Microstructural characterization

The image quality (IQ) map of the PD1-SC sample (Figure 3.7 (a)) reveals elongated grains with sub-grain formation, while the PD1-SCR sample (Figure 3.7 (c)) exhibits a bimodal grain size distribution, featuring fine grain size of 1.9 ± 0.6 μm and coarse grain size measuring 9.8 ± 1.9 μm. The formation of a bimodal grain size distribution in the microstructure can be attributed to processes during cold rolling and subsequent annealing. Cold rolling induces plastic deformation, leading to elongated grains with high dislocation density and increased internal energy, particularly around grain boundaries and sub-grain formations. During annealing at high temperatures for short duration, new, strain-free grains nucleate in high-energy areas, typically at grain boundaries or triple junctions, forming a fine-grain population due to rapid nucleation but restricted growth because of short duration. Some grains, especially those with favorable orientations, grow fast which creates a coarser-grain population. Finally, a stable bimodal grain structure with both fine and coarse grains is produced. The average austenite grain size decreased from 26.74 ± 1.76 μm in the PD1-SC sample (Figure 3.7(b)) to 5 ± 1.51 μm in the PD1-SCR sample (Figure 3.7 (d)), which can be attributed to limited grain growth during repeated annealing.

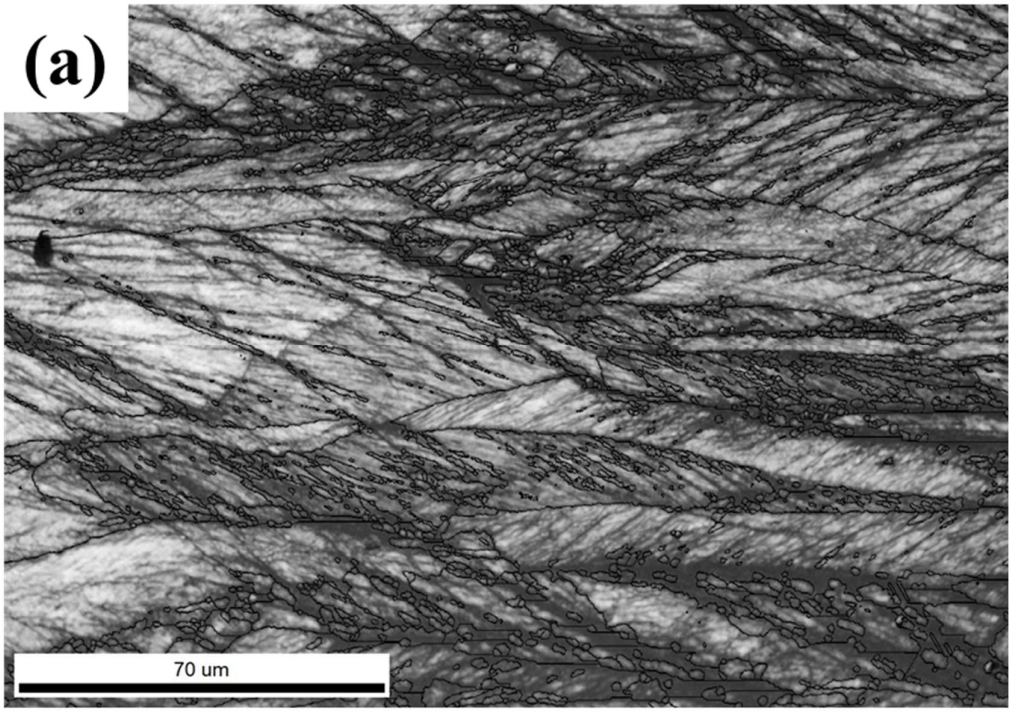
(a)
70 um

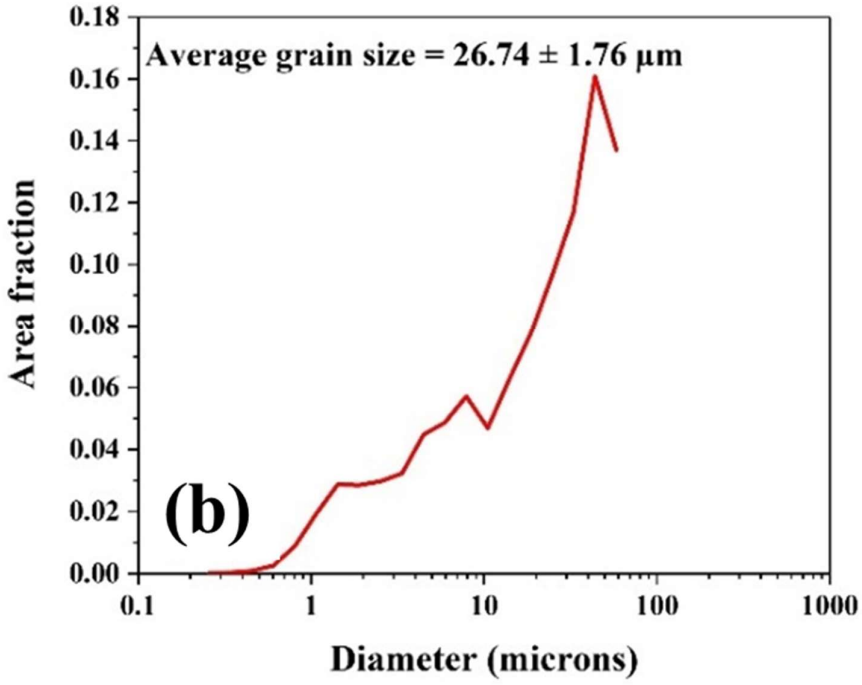
Average grain size = 26.74 ± 1.76 µm
(b)
Area fraction
Diameter (microns)
0.18
0.16
0.14
0.12
0.10
0.08
0.06
0.04
0.02
0.00
0.1
1
10
100
1000

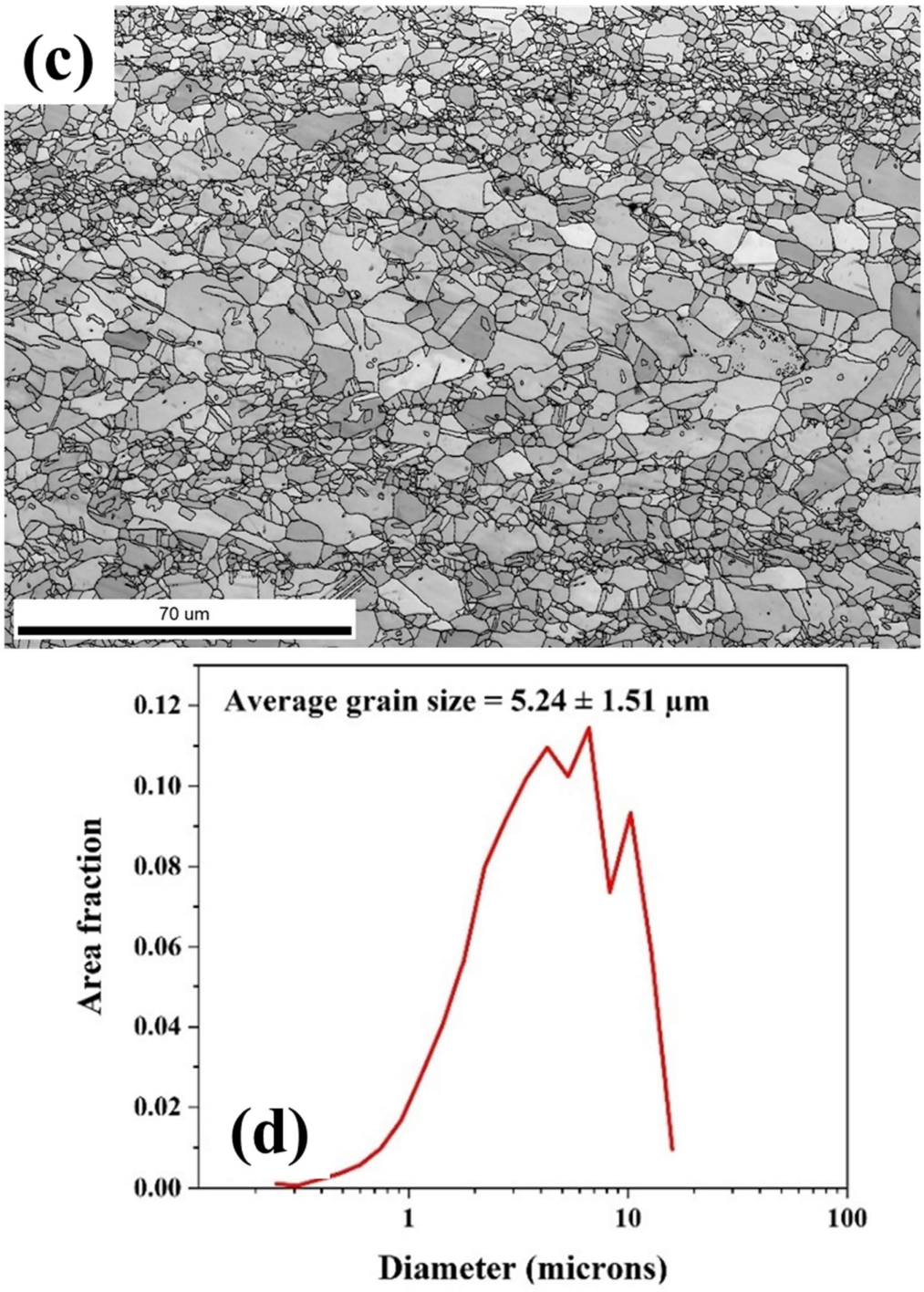

Figure 3.7: IQ maps of (a) PD1-SC and (c) PD1-SCR samples, grain size vs. area fraction charts for (b) PD1-SC, and (f) PD1-SCR samples.

The kernel average misorientation (KAM) maps for the PD1-SC (Figure 3.8 (a)) and PD1-SCR (Figure 3.8 (b)) samples show average KAM values of 1.24° and 0.28°, respectively. The PD1-SC sample exhibits an increase in localized strain distribution due to cold deformation, while the PD1-SCR sample displays a significant reduction in strain distribution, attributed to the recrystallization process. The grain size, dislocation density and KAM values are shown in Table 3.4.

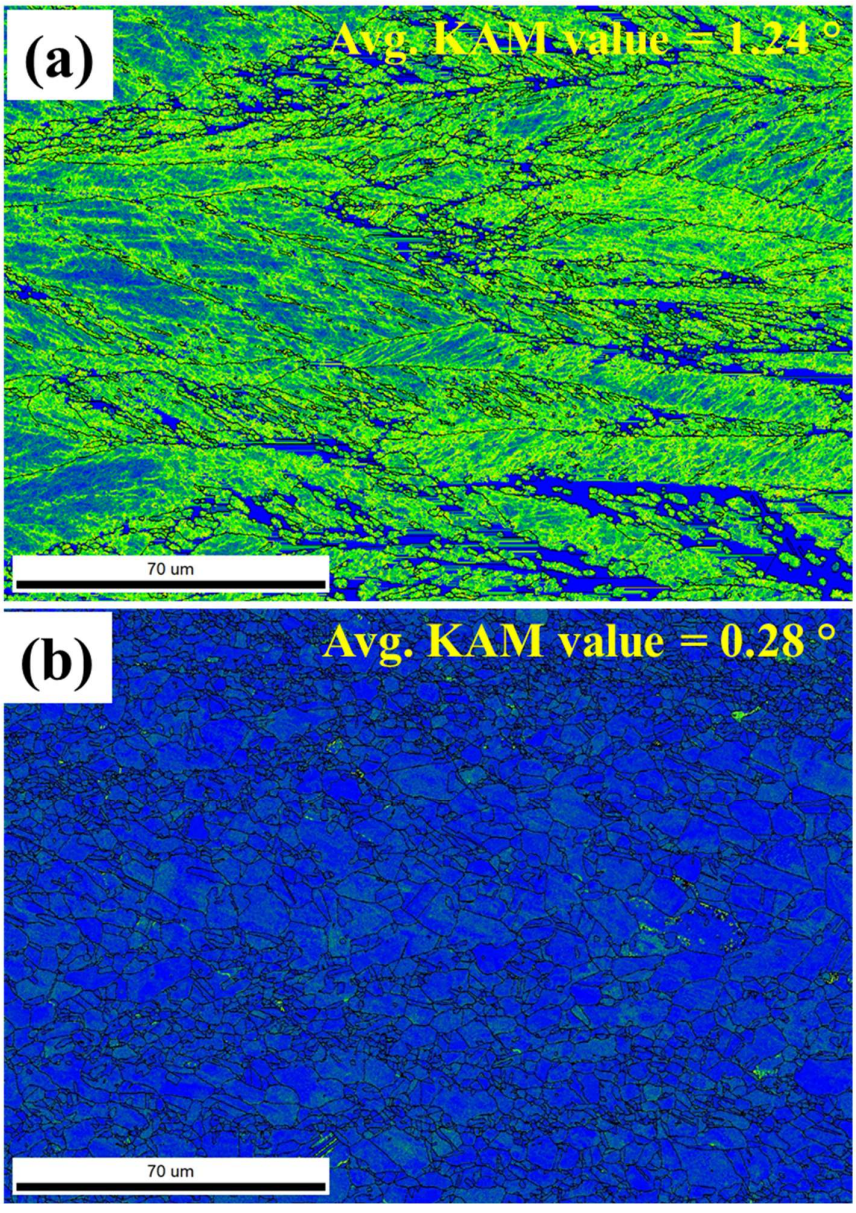

Figure 3.8: KAM maps of (a) PD1-SC and (b) PD1-SCR samples.

Table 3.4: Microstructural data of PD1-SC and PD1-SCR samples.

Material	Grain size (μm)	Dislocation density (10^{14} m^{-2})	KAM value (°)
PD1-SC	26.74 ± 1.76	24	1.24
PD1-SCR	5 ± 1.51	0.92	0.28

The IQ map with superimposed grain boundaries for PD1-SC sample (Figure 3.9 (a)) reveals approximately 89.9% low- angle grain boundaries following cold rolling, with only 10.1% high-angle boundaries. In contrast, the PD1-SCR sample (Figure 3.9 (b)) shows a reduction in low-angle boundaries to 10.1% and an increase in high-angle boundaries to 89.9%, a transformation attributed to the coalescence of low-angle boundaries. At 900°C, sufficient thermal energy enabled boundary movement and coalescence, promoting recrystallization.

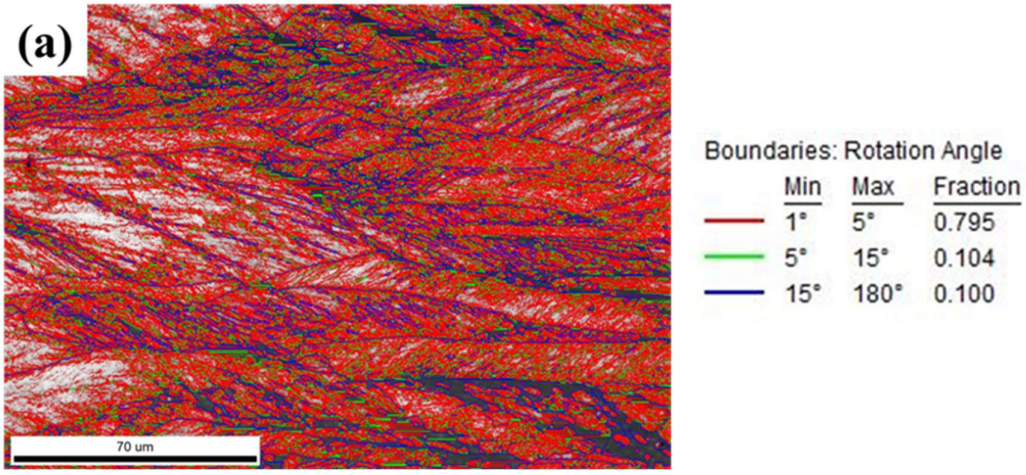

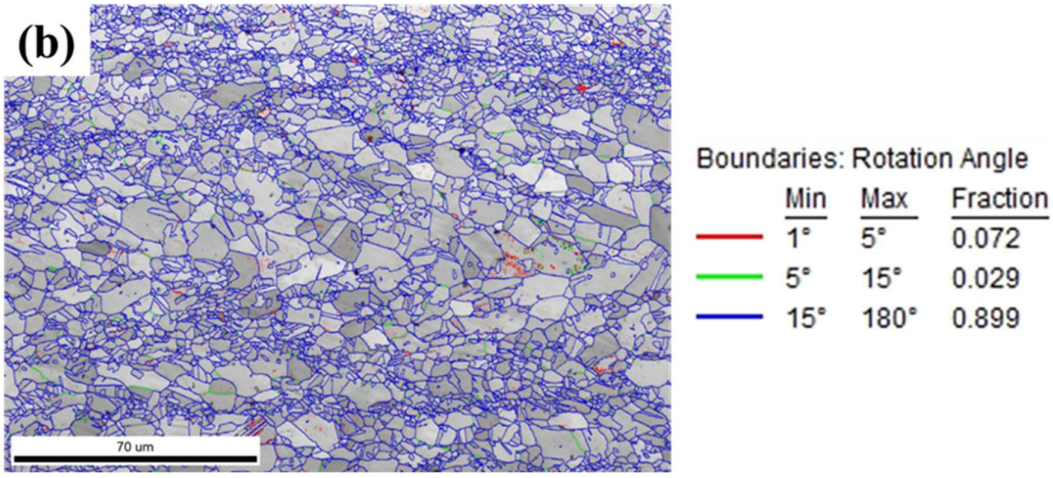

Figure 3.9: IQ maps with superimposed grain boundaries of (a) PD1-SC and, (b) PD1-SCR samples.

Microtexture analysis using the orientation distribution function (ODF) sections at $\varphi_2 = 0°$, 45°, and 65° for the austenite phase in the PD1-SC sample (Figure 3.10 (a)) reveals a maximum shear texture intensity of 7.5 times random in the $\varphi_2 = 65°$ section, indicating a predominant deformation texture. A rotated Goss texture with an intensity of 2.8 R is also observed in the $\varphi_2 = 0°$ section. In the PD1-SCR sample (Figure 3.10 (b)), the shear texture intensity decreases significantly to 1.4 R, while a Goss/Brass texture component (G/B) appears in the $\varphi_2 = 0°$ and $\varphi_2 = 45°$ sections with a maximum intensity of 2.4 R. This corresponds to a 94% reduction in deformation texture compared to the PD1-SC sample, showing minimal deformation texture in the PD1-SCR sample. The dislocation density for both materials was calculated from X-ray diffraction data using the Williamson-Hall equation. The dislocation density values are found to be 24×10^{14} m^{-2} and 0.92×10^{14} m^{-2} for PD1-SC and PD1-SCR samples, respectively.

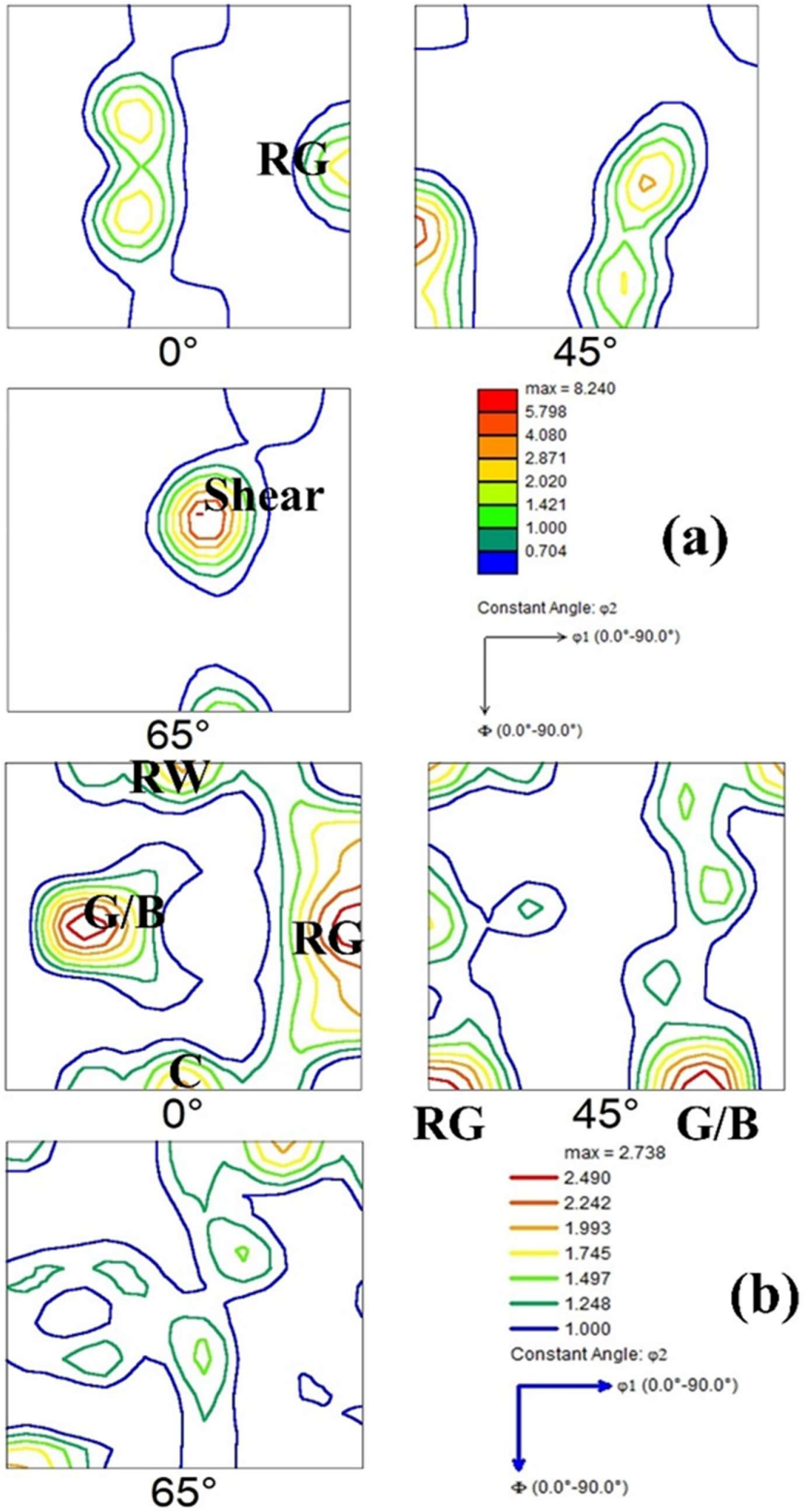

Figure 3.10: φ2 = 0°, 45° and 65° sections of orientation distribution functions (ODFs) of austenite phase in (a) PD1-SC sample and (d) PD1-SCR sample (RG= Rotated Goss, RW= Rotated W).

3.4.1.2 Mechanical properties

Hardness was measured using a Vickers hardness tester with a 1 kgf load, resulting in hardness values of 534 ± 16 VHN for the PD1-SC sample and 312 ± 9 VHN for the PD1-SCR sample. This significant reduction in hardness from the PD1-SC to the PD1-SCR sample is likely attributed to the decrease in dislocation density. The engineering stress – plastic strain curves for PD1-SC and PD1-SCR samples are shown in Figure 3.11 (a). The PD1-SC sample exhibits a yield strength (YS) of 1397 MPa, an ultimate tensile strength (UTS) of 1438 MPa, a plastic elongation (PE) of 4%, and a Tensile toughness (PSE) of 5.75 GPa·%. In contrast, the PD1-SCR sample shows a YS of 635 MPa, UTS of 958 MPa, PE of 50.8%, and PSE of 48.16 GPa·%. The tensile properties are presented in Table 3.5. The engineering stress-strain curves for PD1-SCR samples tested at various strain rates are displayed in Figure 3.11 (b). At a strain rate of 10^{-2} /s, the YS is 899 MPa, the UTS is 1154 MPa, with a PE of 42.9% and tensile toughness of 49.51 GPa·% (Table 3.6). At a strain rate of 10^{-1} /s, the YS increases to 944 MPa, UTS to 1203 MPa, PE decreases to 33.4%, and tensile toughness is 40.5 GPa·% (Table 3.6). Finally, at a strain rate of 10^{0} /s, the YS reaches 1001 MPa, UTS is 1217 MPa, PE is further reduced to 29.9%, with a tensile toughness is 36.8 GPa·% (Table 3.6).

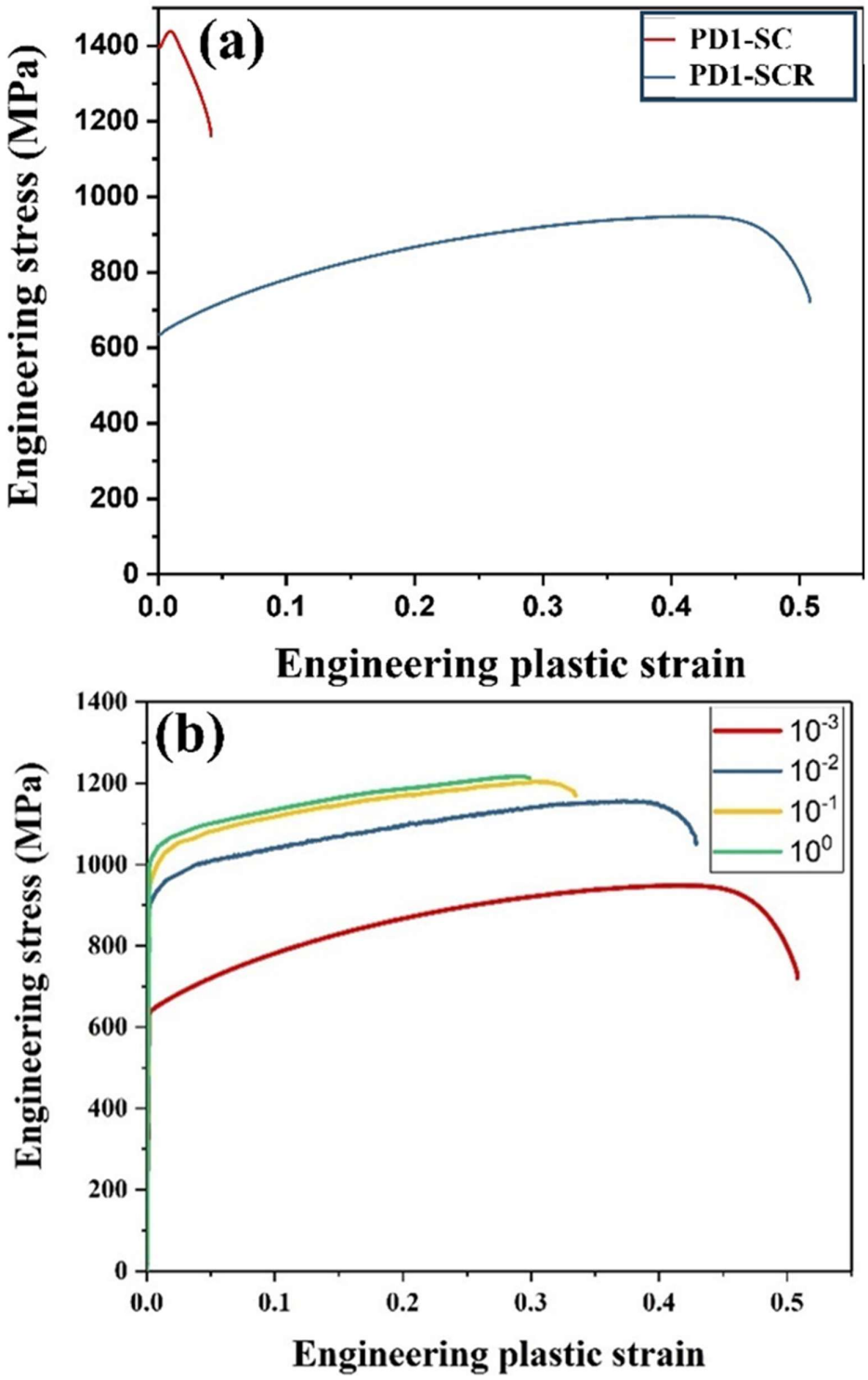

Figure 3.11: Engineering stress-strain curves of (a) PD1-SC, and PD1-SCR samples at 10^{-3}/s strain rate (b) Engineering tensile stress-strain curves for PD1-SCR samples tested at strain rates of 10^{-3}/s, 10^{-2}/s, 10^{-1}/s, 10^{0}/s.

Table 3.5: Tensile properties of PD1-SC and PD1-SCR samples.

Material	YS (MPa)	UTS(MPa)	PE (%)	PSE (GPa. %)
PD1-SC	1397	1438	4	5.75
PD1-SCR	635	958	50.8	48.16

Table 3.6: Tensile properties of PD1-SCR tested at various strain rates.

Strain rate (/s)	YS (MPa)	UTS(MPa)	PE (%)	PSE (GPa. %)
10^{-2}	899	1181	42.9	50.6
10^{-1}	944	1257	33.4	41.9
10^{0}	1001	1262	29.9	37.7

The fractography features are shown in Table 3.7. The fractography of PD1-SCR at a strain rate of 10^{-3} s^{-1} displays a high area percentage of dimples of 67% with a size of 8.4 ± 1.4 µm (Figure 3.12 (a)). The high area percentage of dimples and size recover plastic elongation to 45%. The fracture surfaces of PD1-SCR at strain rates of 10^{-2} s^{-1}, 10^{-1} s^{-1}, and 10^{0} s^{-1}, depict respective dimple area percentages of 61%, 56%, and 41 % with sizes of 6.0 ± 1.5 µm (Figure 3.12 (b)), 4.2 ± 1.5 µm (Figure 3.12 (c)), and 3.7 ± 1.3 µm (Figure 3.12 (d)). The reduced area percentages and size of dimples or increased area fraction of shear fracture reflect the decrease in plastic elongation.

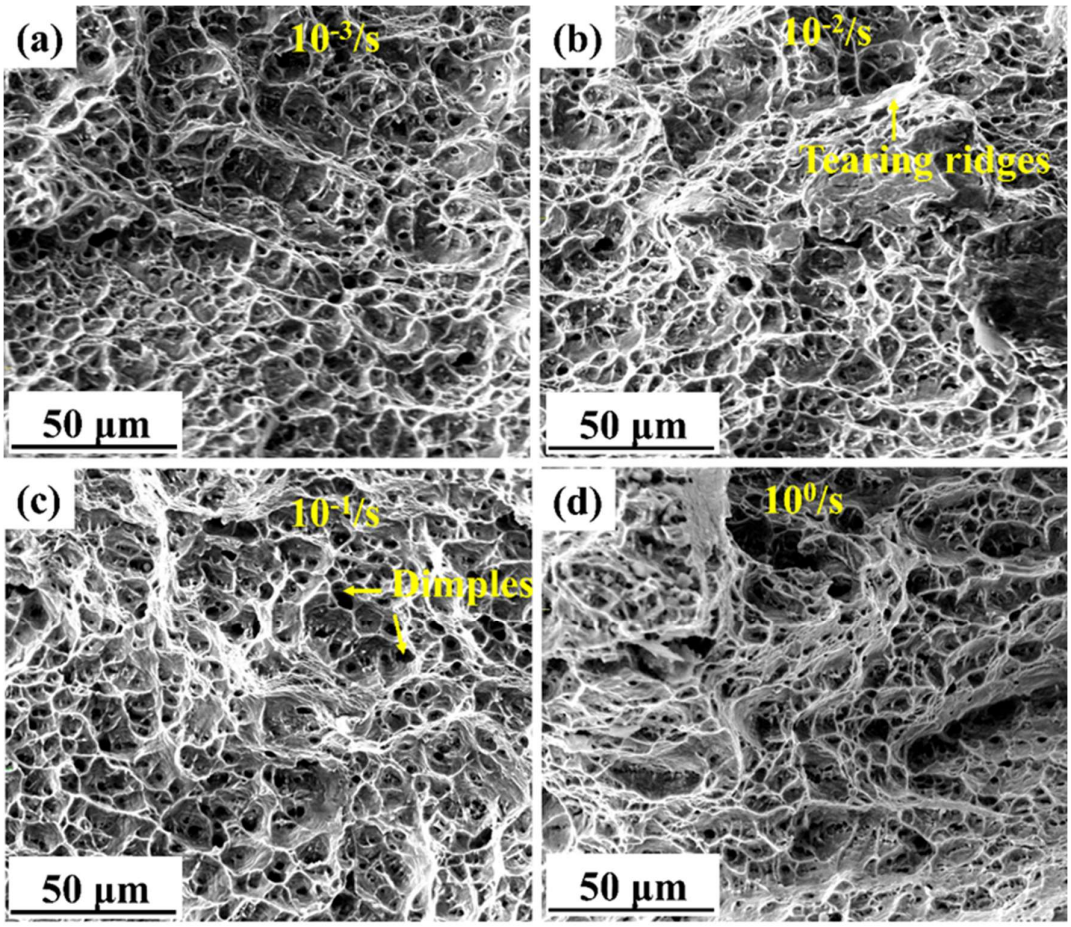

Figure 3.12: Fracture morphologies of PD1-SCR samples tested at strain rates of (a) 10^{-3}/s, (b) 10^{-2}/s, (c) 10^{-1}/s, (d) 10^{0}/s.

Table 3.7: Fractography analysis of PD1-SCR samples at various strain rates.

Strain rate (/s)	Dimple size, (µm)	Dimple area percentage (%)	Facets area fraction (%)
10^{-3}	8.4 ± 1.4	67	33
10^{-2}	6.0 ± 1.5	61	39
10^{-1}	4.2 ± 1.5	56	44
10^{0}	3.7 ± 1.3	41	59

3.4.2 Discussion

The contribution from solid solution and Peierls stress to yield strength in PD1-SC and PD1-SCR samples remain the same as of PD1-S sample which are reported earlier to be 306 MPa and 39 MPa, respectively. Therefore, the difference in yield strength (YS) between these two materials is attributed to dislocation and grain boundary strengthening. On cold rolling the PD1-S sample dislocation density increases but grain size decreases. As a result, the contribution to YS from dislocation density increases to 831 MPa, and the grain boundary strengthens to 66 MPa in PD1-SC sample (Table 3.8).

Table 3.8: Contribution of strengthening mechanisms to yield strength of PD1-SC and PD1-SCR samples.

Material	PD1-SC	PD1-SCR
Contribution to yield strength	(MPa)	(MPa)
Friction stress (σ_P)	39	39
Solid solution strengthening (σ_{ss})	306	306
Dislocation strengthening (σ_{dis})	831	116
Grain boundary strengthening (σ_{gb})	66	178
Calculated yield strength (MPa)	1242	639
Experimental yield strength (MPa)	1397	635

On repeated annealing of the PD1-SC sample, dislocation density decreases drastically in addition to significant refinement of grain size. The contribution to YS from grain boundary increases from 66 MPa to 178 MPa but reduction in dislocation density decreases

its contribution from 831 MPa to 116 MPa in PD1-SCR sample. The experimental YS of the PD1-SC sample displays 155 MPa higher than that of the calculated one. The excess value may be possibly due to the contribution from texture components. The experimental YS of the PD1-SCR sample closely matches that of the calculated one.

3.4.2.1 Work hardening behavior

There are three stages of work hardening, i.e. easy glide (stage I), steady linear work hardening rate (stage II), and dynamic recovery (stage III) observed in PD1-SCR sample but only stage I and stage II were found in PD1-SC sample (Figure 3.13). The work hardening rate for stage I (θ_1) and stage II (θ_2) in PD1-SC sample, are 9711 MPa and 5530 MPa, respectively (Table 3.9). For PD1-SCR sample, the corresponding work hardening values of stage I (θ_1), stage II (θ_2) and stage III (θ_3) are 2633 MPa, 1887 MPa, and 1350 MPa, respectively (Table 3.9). For PD1-SC sample, the transition strains for stage I (ε_1) to stage II is 0.007 and fracture occurs at a true strain of 0.0081. The transition strains corresponding to the end of stages I (ε_1), II (ε_2), and III (ε_3) are 0.087, 0.3008, and 0.3589, respectively, for PD1-SCR.

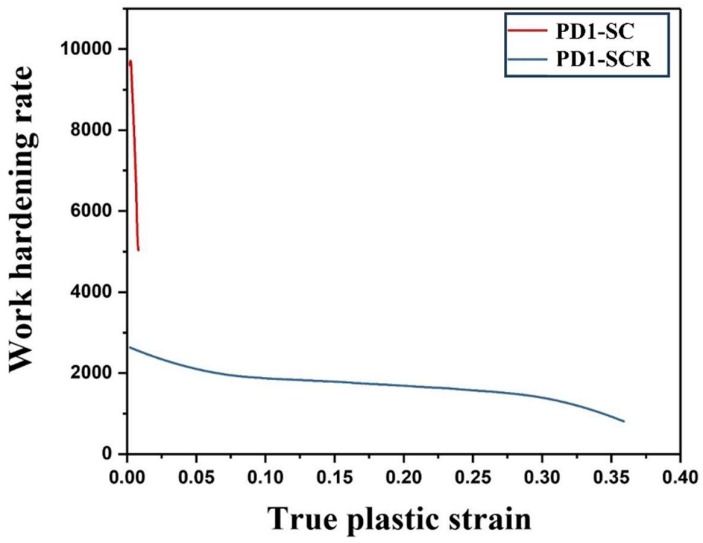

Figure 3.13: Work hardening rate vs true plastic strain diagrams of PD1-SC and PD1-SCR samples.

Table 3.9: Work hardening parameters of PD1-SC and PD1-SCR samples.

Sample	θ_1 (MPa)	θ_2 (MPa)	θ_3 (MPa)	ε_1	ε_2	ε_3
PD1-SC	9711	5530	--	0.007	0.0081	
PD1-SCR	2633	1887	1350	0.087	0.3008	0.3599

The work hardening rate decreases rapidly in stage I with the gradients of -848 GPa, and -9.52 GPa for PD1-SC and PD1-SCR, samples, respectively. The initial sharp drop in work-hardening rate in stage I is due to longer dislocation mean free path is (low dislocation density) to prevent tangling [128]. This stage is observed within the strain range of 0.0-0.007 for PD1-SC and 0.0-0.087 for PD1-SCR. During the initial stage of deformation, the moving dislocations become tangled by the end of stage I and can rearrange into dislocation cell substructures with further straining. The faster decay in the work-hardening rate observed in stage I at higher strain rates is likely due to the more rapid tangling and subsequent rearrangement of dislocations. The higher decreasing work hardening rate in PD1-SC than that of PD1-SCR is due to rapid work hardening caused by the presence of higher dislocation density which was developed earlier in the PD1-SC sample due to cold rolling. As a result, the work-hardening gradient of PD1-SC is much higher than that of PD1-SCR. In stage II, the rate of work hardening decreases gradually within the plastic strain range of 0.007-0.081 and 0.087-0.3008 for PD1-SC and PD1-SCR samples, respectively. In Stage II, the activation of cross-slip and multiple-slip systems facilitates the formation of heterogeneous dislocation structures. This stage corresponds to enhanced dislocation storage, as suggested by the proliferation of walls and cell structures. Consequently, there is an increase in dislocation density. The work hardening rate

decreases with a gradient of -440 GPa in PD1-SC and -1.9 GPa in PD1-SCR. Stage III represents the dynamic recovery phase, wherein dislocations undergo annihilation, leading to a reduction in the work hardening rate. The linear relationship observed between the hardening rate ($\frac{d\sigma}{d\epsilon_p}$) and true plastic stress (σ) curves in the third stage can be most effectively elucidated similar to the Kock, Mecking, (KM) dislocation models as expressed in Equation 3.7. The dislocation storage capacity (θ_0) of PD1-SCR is determined to be 6138 MPa, and the negative slope (m) of the curve for PD1-SCR is observed to be -3.77, respectively.

In the PD1-SC sample, the highest work hardening rate but restricted plastic elongation of 0.8% provides a low amount of hardening of only 41 MPa. Despite low hardening, the material reports the highest tensile strength of 1438 MPa because of the highest yield strength. The presence of a higher volume fraction of fine grains in PD1-SCR provides higher work hardening in combination with high plastic elongation providing to maximum increase in strength of 323 MPa to achieve a high ultimate tensile strength of 958 MPa.

The presence of highest dislocation density in PD1-SC sample restricts the plastic elongation to 0.8%. Repeated annealing of the PD1-SC sample for a short time leads to refinement in grain size by recrystallization and reduces dislocation density to a low value which increases plastic elongation to 51%.

3.5 Conclusions

- Addition of 6.2 mass% Al in selected austenitic steel reduces density to 6.99 g/cc.
- Repeated annealing of coarse-grained cold-rolled austenitic low-density steel for a short time above the recrystallization temperature, followed by water quenching, leads to a refinement to 1.3-11.7 μm range with a bimodal distribution of 53.7% fine grains of 1.9 μm size and 46.3 % coarse grains of 9.8 μm size.

- Short annealing of PD1-SC sample at 900°C for just 120 s reduces localized strain, and dislocation density, produces relatively strain-free crystal by recrystallization, and increases high-angle boundary area percentage to 89%.
- The short annealing of the PD1-SC sample reduces deformation texture components drastically and develops recrystallization texture.
- PD1-SC sample reports the highest yield strength of 1397MPa due to high dislocation density and limited plastic elongation of 0.8% in the uniform deformation range. Repeated annealing reduces yield strength to 635 MPa but recovers plastic elongation to 45%. Strengthening of the PD1-SC sample is dominated by contribution from dislocation but the yield strength of the PD1-SCR sample is mainly controlled by grain refinement.
- The work hardening of PD1-SC exhibits only easy glide and steady linear work hardening rate due to rapid strain-induced hardening and a high initial dislocation density from cold rolling, while PD1-SCR sample display three stages of work hardening i.e. additional stage of dynamic recovery though finer-sized PD1-SCR displayed higher dislocation storage and lower dynamic recovery.
- The PD1-SC sample, with the highest work hardening rate but limited elongation of 0.8%, shows a modest hardening of only 41 MPa, yet achieves the highest tensile strength of 1438 MPa due to its elevated yield strength. The PD1-SCR sample, with a higher fraction of fine grains, combines increased work hardening with significant elongation, leading to an UTS of 958 MPa.
- PD1-SCR sample recovers plastic elongation by bimodal grain size distribution maintaining high strength as a result of refinement.
- The increase in strain rate leads to the formation of smaller dimples and a higher amount of shear fracture and tear zones that result in loss of plastic elongation.